Investigation on the Interface Characteristics of Al/Mg Bimetallic Castings Processed by Lost Foam Casting

WENMING JIANG, GUANGYU LI, ZITIAN FAN, LONG WANG, and FUCHU LIU

The lost foam casting (LFC) process was used to prepare the A356 aluminum and AZ91D magnesium bimetallic castings, and the interface characteristics of the reaction layer between aluminum and magnesium obtained by the LFC process were investigated in the present work. The results indicate that a uniform and compact interface between the aluminum and magnesium was formed. The reaction layer of the interface with an average thickness of approximately 1000 μm was mainly composed of Al_3Mg_2 and $Al_{12}Mg_{17}$ intermetallic compounds, including the Al_3Mg_2 layer adjacent to the aluminum insert, the $Al_{12}Mg_{17}$ middle layer, and the $Al_{12}Mg_{17}$ + δ eutectic layer adjacent to the magnesium base. Meanwhile, the Mg_2Si intermetallic compound was also detected in the reaction layer. An oxide film mainly containing C, O, and Mg elements generated at the interface between the aluminum and magnesium, due to the decomposed residue of the foam pattern, the oxidations of magnesium and aluminum alloys as well as the reaction between the magnesium melt and the aluminum insert. The microhardness tests show that the microhardnesses at the interface were obviously higher than those of the magnesium and aluminum base metals, and the Al_3Mg_2 layer at the interface had a high microhardness compared with the $Al_{12}Mg_{17}$ and $Al_{12}Mg_{17}$ + δ eutectic layers, especially the eutectic layer.

I. INTRODUCTION

ALUMINUM and magnesium alloys are regarded as the most important engineering materials in automotive and aerospace industries because of their many advantages including low density, high strength-to-weight ratio, and excellent castability.[1–4] However, one of these materials alone does not satisfy the requirements of lightweight constructions in many cases, for instance, magnesium alloy suffers from low ductility, creep resistance, and high-temperature strength, while aluminum alloy can satisfy these, particularly in the automotive industry.[5–7] Using combined structures consisting of aluminum and magnesium alloys as the bimetallic materials may be the most effective way to meet the demands for engineering applications because they combine several promising properties that cannot be provided by monolithic materials.[8]

The LFC process is a cost-effective and environment-friendly near-net-shape casting technology without the need for cores,[9–11] and suitable for manufacturing complicated aluminum and magnesium alloys' precision castings.[12,13] First, the foam pattern based on the part shape is prepared. Subsequently, the prepared foam pattern is coated with the refractory slurry and then placed inside a sand flask. After modeling and vibration compacting, the molten metal is poured directly into the foam pattern, thereby decomposing the foam pattern as gas and liquid products. As a consequence, the molten metal replaces the foam pattern and duplicates all features of the foam pattern.[14] Currently, an interesting advantage of the LFC process is the possibility of mounting the desired solid part inside the foam pattern and then performing the pouring process, which will be an attractive method to prepare the bimetallic castings because it has numerous advantages, such as low cost, no cores, tight tolerance, complex geometries, and smooth as-cast surface. A number of researchers have carried out such tries. Hejazi et al.[15] investigated the effect of copper insert on the microstructure of gray iron produced via LFC process. Divandari et al.[16] reported the study of Al/Cu rich phases formed in A356 alloy by inserting Cu wire in pattern in LFC process. Choe et al.[17] studied the interface between steel insert and aluminum casting in LFC process.

There are many methods to fabricate Al/Mg bimetallic materials, for example, compound casting based on sand casting,[18] friction stir welding,[19] electro polishing

WENMING JIANG, Associate Professor, is with the State Key Lab of Materials Processing and Die and Mould Technology, Huazhong University of Science and Technology, Wuhan 430074, P.R. China, and also with the School of Mechanical & Electrical Engineering, Wuhan Institute of Technology. ZITIAN FAN, Professor, and GUANGYU LI, LONG WANG and FUCHU LIU, Graduate Students, are with the State Key Lab of Materials Processing and Die and Mould Technology, Huazhong University of Science and Technology. Contact e-mail: fanzt@hust.edu.cn

+ anodizing surface treatment method,[20] vacuum diffusion bonding,[21] and laser welding.[22] However, only few literatures reported that the Al/Mg bimetallic castings are obtained by the LFC process. Emami et al.[23] prepared the pure aluminum and magnesium light metals using the LFC process. Guler et al.[24] fabricated the A319 aluminum and AM50 magnesium bimetal using the LFC process. Therefore, the knowledge with respect to the interface investigation of reaction layer between the aluminum and magnesium alloys is still incomplete in the fabrication of the Al/Mg bimetallic materials processed by the LFC process.

In the present work, the LFC process was employed to produce the A356 aluminum and AZ91D magnesium bimetallic castings, and the interface characteristics of the reaction layer between the solid aluminum insert and the molten magnesium melt obtained by the LFC process were investigated. The objective of the present work is to prepare the Al/Mg bimetallic castings using the LFC process and to reveal the interface characterization and formation mechanism of the reaction layer between the aluminum and magnesium alloys.

II. EXPERIMENTAL PROCEDURES

A. Materials

The expandable polystyrene (EPS) foam materials were used to fabricate the foam pattern with a density of 0.025 g/cm³ using a foaming molding process. The foam pattern was then dipped in a water-based refractory slurry and allowed to dry.

A356 aluminum and AZ91D magnesium alloys were used to prepare the Al/Mg bimetallic castings, which were used as a substrate material and a molten magnesium bath, respectively. Chemical compositions of the A356 aluminum and AZ91D magnesium alloys used are listed in Table I.

A cylindrical A356 aluminum alloy insert with a 14 mm diameter and a 130 mm height was machined from an A356 aluminum alloy ingot using an electrical discharge machine. Next, the cylindrical A356 aluminum insert was ground with silicon carbide papers up to 1200 grit, and then rinsed using 10 pct sodium hydroxide solution, 0.5 mol/l hydrochloric acid and ethanol, respectively. The prepared cylindrical A356 aluminum insert was subsequently mounted inside the foam pattern.

B. Casting Process

Figure 1 presents a schematic illustration of experimental equipment of the LFC process. The prepared foam pattern together with the A356 aluminum insert was first placed in a sand flask. The sand flask was then filled with unbonded loose-sand and compacted using a vibration table. Prior to pouring process, the sand flask was covered with a plastic film.

A stainless steel crucible was first preheated at 573 K (300 °C) in an electrical resistance furnace. The preheated AZ91D magnesium alloy ingots were then placed inside the stainless steel crucible to melt under the CO_2-0.5 pct SF_6 protective gas mixture. When the temperature of the molten metal reached 1003 K (730 °C), the slag of the molten metal was skimmed. Afterwards, the vacuum pump was started to exhaust air from the sand flask and obtain a vacuum pressure of 0.03 MPa in the sand flask, and the molten metal was then poured into the foam pattern with a temperature of 1023 K (750 °C). During the pouring process, the vacuum pressure of the sand flask was always maintained at 0.03 MPa. Finally, the Al/Mg bimetallic castings were obtained after pouring and solidification.

C. Interface Microstructural Characterizations

In order to investigate interfacial microstructures of the Al/Mg bimetallic castings obtained by the LFC process, metallographic samples were cut from the bimetallic castings using the electrical discharge machine. Subsequently, the metallographic cross-sections were prepared by grinding and polishing, and then etched using a 0.5 pct hydrofluoric acid solution. The interfacial microstructures of the metallographic samples were observed using an Me F-3 metallographic microscope or a Quanta 400 scanning electron microscope (SEM; FEI Corporation, Hillsboro, OR). The compositional variations of reaction layers at the interface were identified using an energy-dispersive
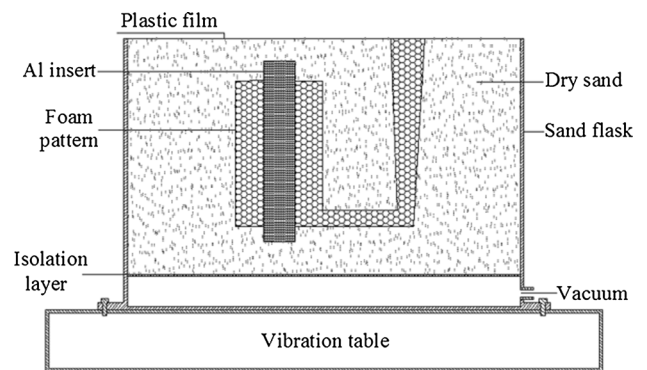

Fig. 1—Schematic illustration of the experimental equipment.

Table I. Nominal Chemical Compositions of the A356 Aluminum and AZ91D Magnesium Alloys (Weight Percent)

Alloy	Composition								
	Al	Zn	Mn	Si	Fe	Cu	Ni	Ti	Mg
A356	balance	—	—	6.75	0.084	—	—	0.14	0.63
AZ91D	8.96	0.8	0.28	0.07	0.039	0.024	8.96	—	Balance

X-ray spectroscopy (EDS) analysis attached to the SEM. The EDS line scan analysis of the interfacial microstructure was used to detect the diffusions of different elements at the interface. The magnification of the SEM micrograph used by the EDS line scan analysis was 100 times. The EDS line scan analysis was recorded by approximately 1720 μm for about 6 minutes. All the intermetallic compounds at the interface were carefully analyzed by the results of several EDS point analyses, which were then estimated by the chemical compositions in such analysis. The magnifications of the SEM micrographs used by the EDS point analyses were 1000 times. The resolutions for all the SEM micrographs were 1024×884. An accelerating voltage of 20 kV and a spot size of approximately 3.5 as well as a working distance of about 12.4 mm were utilized for the EDS analysis. Phase analyses at the interface of the Al/Mg bimetal castings were performed to confirm the presence of intermetallic compounds using an X-ray diffractometry (XRD) analysis with Cu K$_\alpha$ radiation.

In addition, an HV-1000 hardness tester was employed to examine the microhardness distributions at the interface zone of the Al/Mg bimetallic castings. The load and holding time of the microhardness tests were 300 g and 10 seconds, respectively.

III. RESULTS AND DISCUSSION

A. Interfacial Microstructures and Composition Analysis

The optical micrographs in Figure 2 show interfacial microstructures of the Al/Mg bimetallic castings obtained by the LFC process. It is evident that a uniform interface consisting of different reaction layers between the aluminum and magnesium is observed, and the average thickness of the reaction layer reaches approximately 1000 μm, as shown in Figure 2(a). Figure 2(b) shows a high-magnitude optical micrograph of interfacial microstructure of the Al/Mg bimetallic castings. As can be seen, the interface between the aluminum and magnesium is free from porosities, and the interfacial microstructure exhibits different microstructure morphologies for the different reaction layers.

Figure 3 shows the SEM micrograph and EDS analysis of interfacial microstructures of the Al/Mg bimetallic castings obtained using LFC process. The SEM micrograph also indicates that a relative uniform and compact interface with different reaction layers is formed between the aluminum and magnesium, as shown in Figure 3(a). According to the EDS line scan analysis of the interfacial microstructure in Figure 3(b), it can be found that the diffusions of Al and Mg elements obviously fluctuate at the interface, where the content of the Mg element gradually decreases across the interface from the magnesium base side toward the aluminum insert, while the diffusion of the Al element presents a contrary law. The diffusions of the Zn and Si elements at the interface are also observed. Moreover, the concentration of the O element is detected adjacent to the middle zone of the interface.
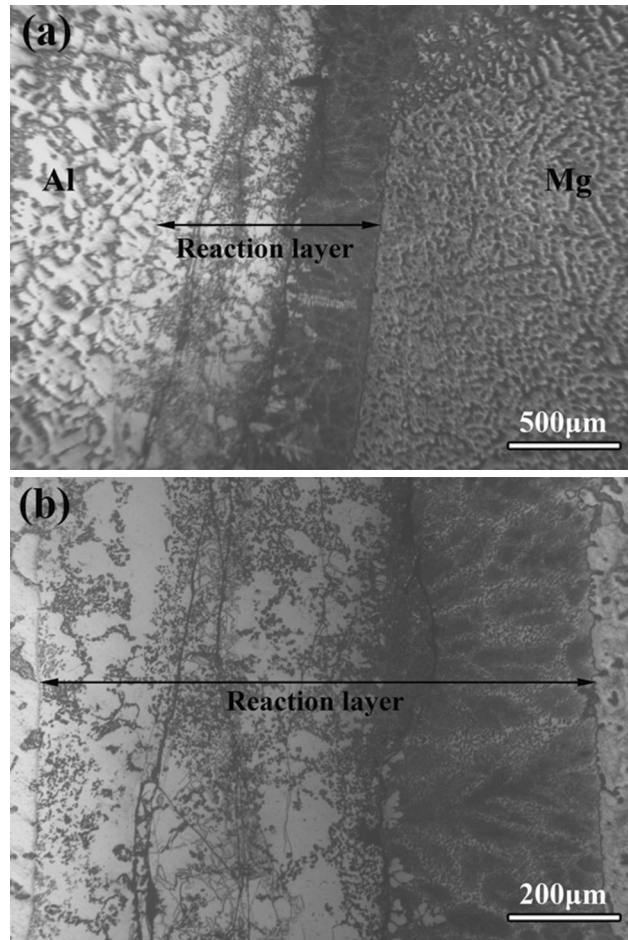

Fig. 2—Optical micrographs of the interfacial microstructures of the Al/Mg bimetallic castings obtained using LFC process: (a) low-magnitude optical micrograph and (b) high-magnitude optical micrograph.

The quantitative analysis results of distributions of the Al and Mg elements using the EDS analysis method at seven different points indicated in Figure 3 are listed in Table II. In terms of the results of the EDS analysis as well as the Al-Mg phase diagram (as shown in Figure 4), it suggests that the reaction layer is mainly composed of Al$_3$Mg$_2$ and Al$_{12}$Mg$_{17}$ intermetallic compounds, including three different layers as follows. The layer I consists of the Al$_3$Mg$_2$ intermetallic compound adjacent to the aluminum insert, the layer II consists of the Al$_{12}$Mg$_{17}$ intermetallic compound in the middle of interface, and the layer III is the eutectic structure (Al$_{12}$Mg$_{17}$ + δ) adjacent to the magnesium base, which are in agreement with the results of other reports.[26,27] In order to further demonstrate the interfacial microstructures of the Al/Mg bimetallic castings, more detailed observations and compositional analysis were performed on the areas B and C in Figure 3(a), as shown in Figure 5. Figures 5(a) through (c) show the morphologies and compositions of the Al$_3$Mg$_2$ and Mg$_2$Si intermetallic compounds at the interface, respectively; meanwhile, the detailed observations and compositional analysis of the eutectic structure consisting of Al$_{12}$Mg$_{17}$ and δ phases at the interface

are exhibited in Figures 5(d) through (f). Figure 5(d) clearly shows the morphologies of the δ (Mg) phase and the $Al_{12}Mg_{17}$ phase in the eutectic structure, and their EDS composition analyses are shown in Figures 5(e) and (f), respectively. These results also mean that the reaction layer is mainly composed of the Al_3Mg_2 and $Al_{12}Mg_{17}$ intermetallic compounds, which are consistent with the results of Table II.

In addition, the X-ray diffraction of the constitutive phases on the interface of the Al/Mg bimetallic castings was also carried out to confirm the presence of the Al_3Mg_2 and $Al_{12}Mg_{17}$ intermetallic compounds, as shown in Figure 6, whereas the Mg_2Si intermetallic compound has not been detected in the X-ray diffraction pattern because of its few quantities.

The formation of reaction layers between the aluminum insert and the magnesium melt is mainly attributed to the interdiffusion of aluminum and magnesium.[8] In the present investigation, two metallic materials that is aluminum and magnesium—one in solid state (A356 aluminum alloy) and the other liquid state (AZ91D magnesium alloy)—are brought into contact with each other in such a manner that a diffusion reaction zone forms between the two materials and thus a continuous metallic transition occurs from one metal to the other. During the casting process, the heat capacity of the magnesium melt first makes the surface of the aluminum insert melt, and the concentration gradient then results in the aluminum and magnesium melts to diffuse into each other. Based on the Al-Mg phase diagram (Figure 4), the Al_3Mg_2 and $Al_{12}Mg_{17}$ intermetallic compounds finally form at the reaction interface between the aluminum and the magnesium. The eutectic structure ($Al_{12}Mg_{17} + \delta$) generates through the $L \longrightarrow Al_{12}Mg_{17}+\delta$ eutectic transformation at 710 K (437 °C). The formation of the Mg_2Si intermetallic compound is mainly due to the contact and reaction between the magnesium melt and the silicon phase existing on the surface layer of the aluminum insert, and the formed Mg_2Si intermetallic compound gradually disperses throughout the interface between the aluminum and magnesium.[18]

B. Oxide Film

In general, the presence of oxide films on the surface between the aluminum and magnesium alloys is always one of the major problems for different preparation methods of the Al/Mg bimetal. In the present investigation, an oxide film is also found at the interface between the aluminum and magnesium. Figure 7 shows
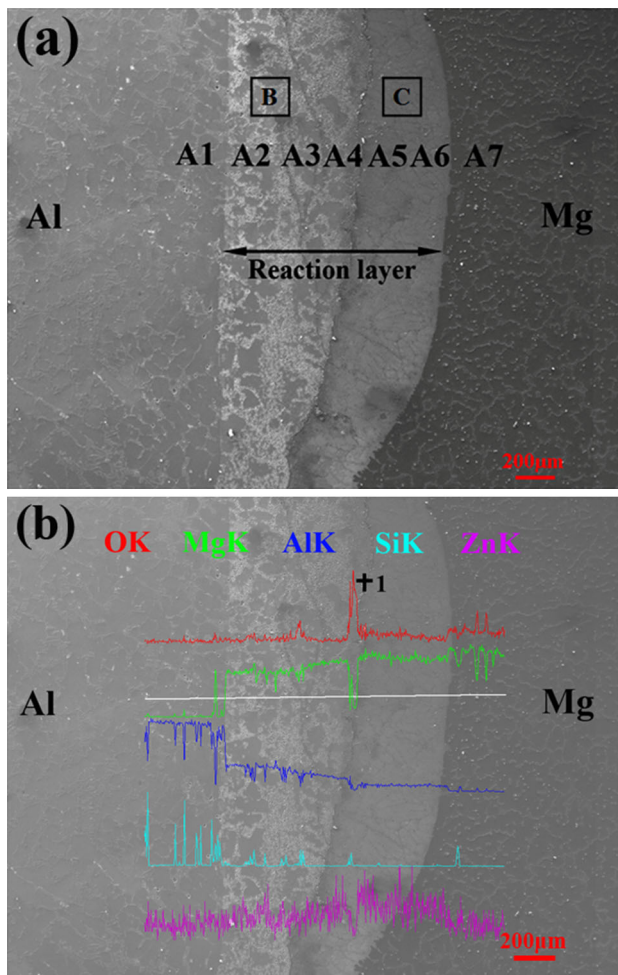

Fig. 3—SEM micrograph and EDS analysis of the interfacial microstructures of the Al/Mg bimetallic castings obtained using LFC process: (a) SEM micrograph and (b) EDS line scan.

Table II. Results of EDS Analysis Corresponding to the Points Indicated in Figure 3

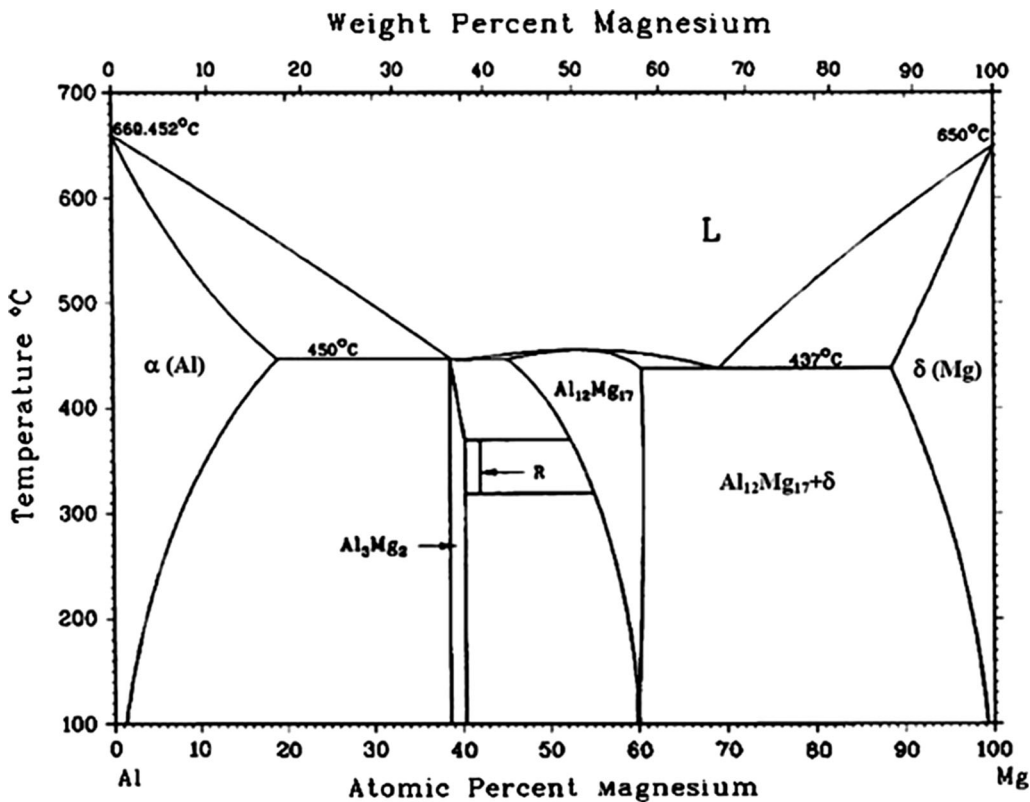| Number | Layer Code | Element Compositions (at. pct) | | Element Composition Ratio (Al/Mg) | Inference Component |
		Al	Mg		
A1	—	100	0	—	Al
A2	I	56.59	40.88	1.38	Al_3Mg_2
A3	II	50.36	47.54	1.06	$Al_{12}Mg_{17}$
A4	II	37.17	55.9	0.66	$Al_{12}Mg_{17}$
A5	III	31.03	68.21	0.45	$Al_{12}Mg_{17} + \delta$
A6	III	30.21	69.35	0.44	$Al_{12}Mg_{17} + \delta$
A7	—	12.58	85.76	0.15	Mg

Fig. 4—Al-Mg phase diagram.[8,25]

the EDS analysis of interfacial microstructures of the Al/Mg bimetallic castings corresponding to the point 1 shown in Figure 3(b), suggesting that the oxide film mainly containing C, O, and Mg elements, especially the C element, generates at the interface between the aluminum and magnesium. Furthermore, the EDS analysis of the interfacial microstructure in Figure 3(b) also indicates the concentration of the O element at the interface.

The formation mechanism of the oxide film can be explained by the following fact. On the one hand, the EDS analysis presents that the content of the C element is the most in the oxide film, which can be inferred that the C element most probably comes from the foam materials during the preparation of the Al/Mg bimetallic castings obtained using the LFC process. That is because the foam pattern employed by the LFC process will decompose plenty of gas and liquid products during the pouring process. Unfortunately, the decomposed residue of the foam pattern cannot escape through the coating layer, which will lead to the generation of the inclusion oxide film defect,[28] as shown in Figure 8. Consequently, the decomposed residue of the foam pattern materials have a significant effect on the formation of the oxide film.

On the other hand, it is well known that both magnesium and aluminum alloys are easy to oxidize during the casting process due to their high affinities to

react with oxygen, resulting in the formation of MgO and Al_2O_3 oxide films.[29–31] Moreover, it is also pointed out that the reaction between the magnesium melt and the aluminum insert can form the oxide film.[18] Hence, the formation mechanism of the oxide film is complex in the case of the present study, and a larger number of factors may be responsible for the formation of the oxide film. Besides, it should be indicated that the oxide film at the interface may prevent the diffusion and chemical reaction processes between the aluminum and magnesium, thereby decreasing the thickness of the reaction layer.

C. Microhardness

Figure 9 represents the microhardness distributions at the interface zone of the Al/Mg bimetallic castings obtained using the LFC process. Figure 10 shows the optical micrographs of interfacial microstructures of the Al/Mg bimetallic castings after microhardness testing. As can be seen in Figure 9, the microhardnesses at the interface are obviously higher than those of the magnesium and aluminum base metals. The microhardnesses at the interface range from 120 to 163 HV, depending on the positions of the indenter relative to the interface location. In comparison, the average microhardnesses of the magnesium base metal and the aluminum base metal are 54 and 45
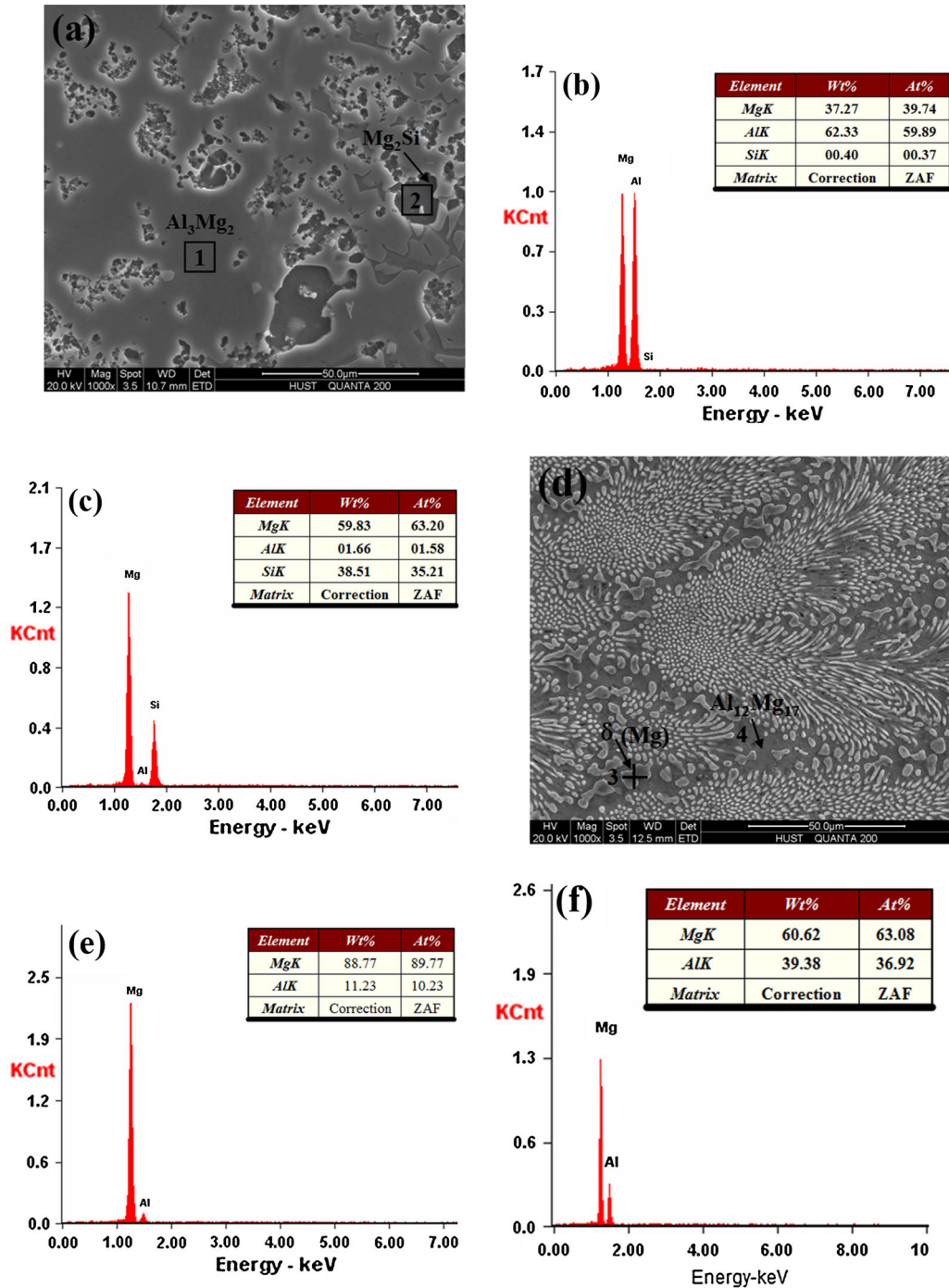
Fig. 5—SEM micrograph and EDS analysis of the interfacial microstructures of the Al/Mg bimetallic castings obtained using LFC process taken from different areas shown in Figure 3(a): (*a*) area marked B; EDS of (*b*) area 1 and (*c*) area 2 marked in (a); (*d*) area marked C; EDS of (*e*) area 3 and (*f*) area 4 marked in (d).

HV, respectively. A higher microhardness at the interface, compared with the magnesium base metal and the aluminum base metal, also implies that the Al-Mg intermetallic compounds have been formed at the interface between the aluminum and the magnesium.[32,33]

Additionally, it can also be observed that the microhardness at the layer I (Al_3Mg_2 intermetallic compound) adjacent to the aluminum insert is the highest than those of the layer II ($Al_{12}Mg_{17}$ intermetallic compound) in the middle of interface and the layer III ($Al_{12}Mg_{17}$ + δ eutectic structure) adjacent to the magnesium base,
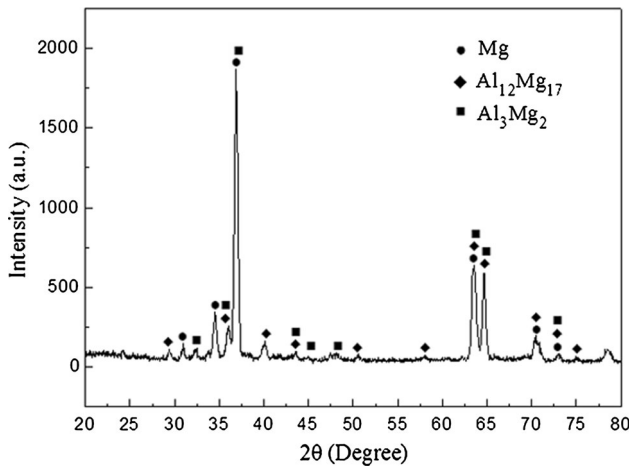
Fig. 6—X-ray diffraction pattern of the constitutive phases on the interface of the Al/Mg bimetallic castings.

while the $Al_{12}Mg_{17}$ + δ eutectic has a relatively lower microhardness because of the presence of the Mg solid solution compared to the Al_3Mg_2 and $Al_{12}Mg_{17}$ intermetallic compounds. These investigations are consistent with the results of other researchers.[8,23,34] Furthermore, Figure 10 clearly shows the indentation sizes at different reaction layers to better demonstrate the microhardness variations of different intermetallic compounds, suggesting that the indentation sizes of the magnesium and aluminum base metals are larger than those of the Al_3Mg_2 and $Al_{12}Mg_{17}$ intermetallic compounds. In addition, it is worth noting that a reaction layer with an excessive thickness between the aluminum and the magnesium will greatly increase the brittleness of the Al/Mg bimetallic castings and weaken the bonding strength of the bimetallic castings.[35,36] Nevertheless, an appropriate brittle interface between the aluminum and the magnesium may be useful to the recycling of the Al/Mg bimetallic castings at the end of the component's life because most of the Al alloy can easily separate from the Mg alloy by a mechanical crushing method. Therefore, our future work will focus on the control of the reaction layers according to the

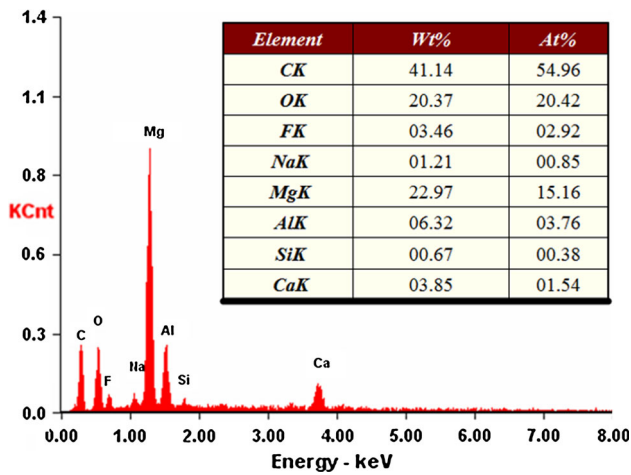| Element	Wt%	At%
CK	41.14	54.96
OK	20.37	20.42
FK	03.46	02.92
NaK	01.21	00.85
MgK	22.97	15.16
AlK	06.32	03.76
SiK	00.67	00.38
CaK	03.85	01.54

Fig. 7—EDS analysis of the interfacial microstructures of the Al/Mg bimetallic castings obtained using LFC process taken from the point 1 shown in Figure 3(b).
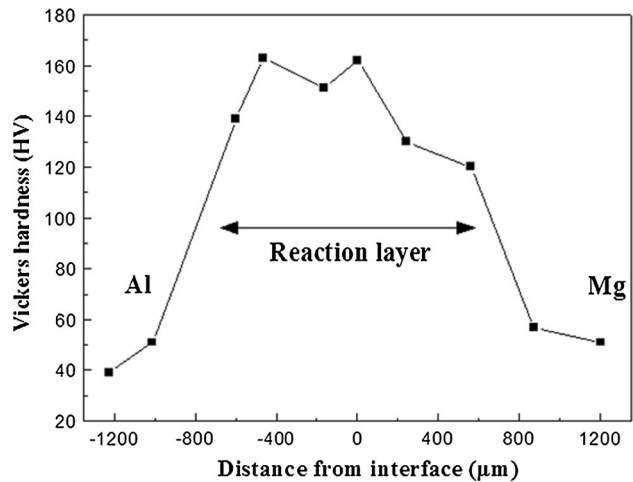

Fig. 9—Microhardness distributions at the interface zone of the Al/Mg bimetallic castings obtained using LFC process.
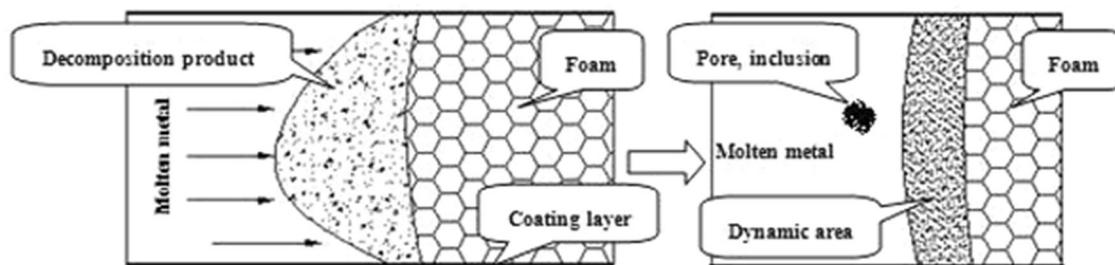

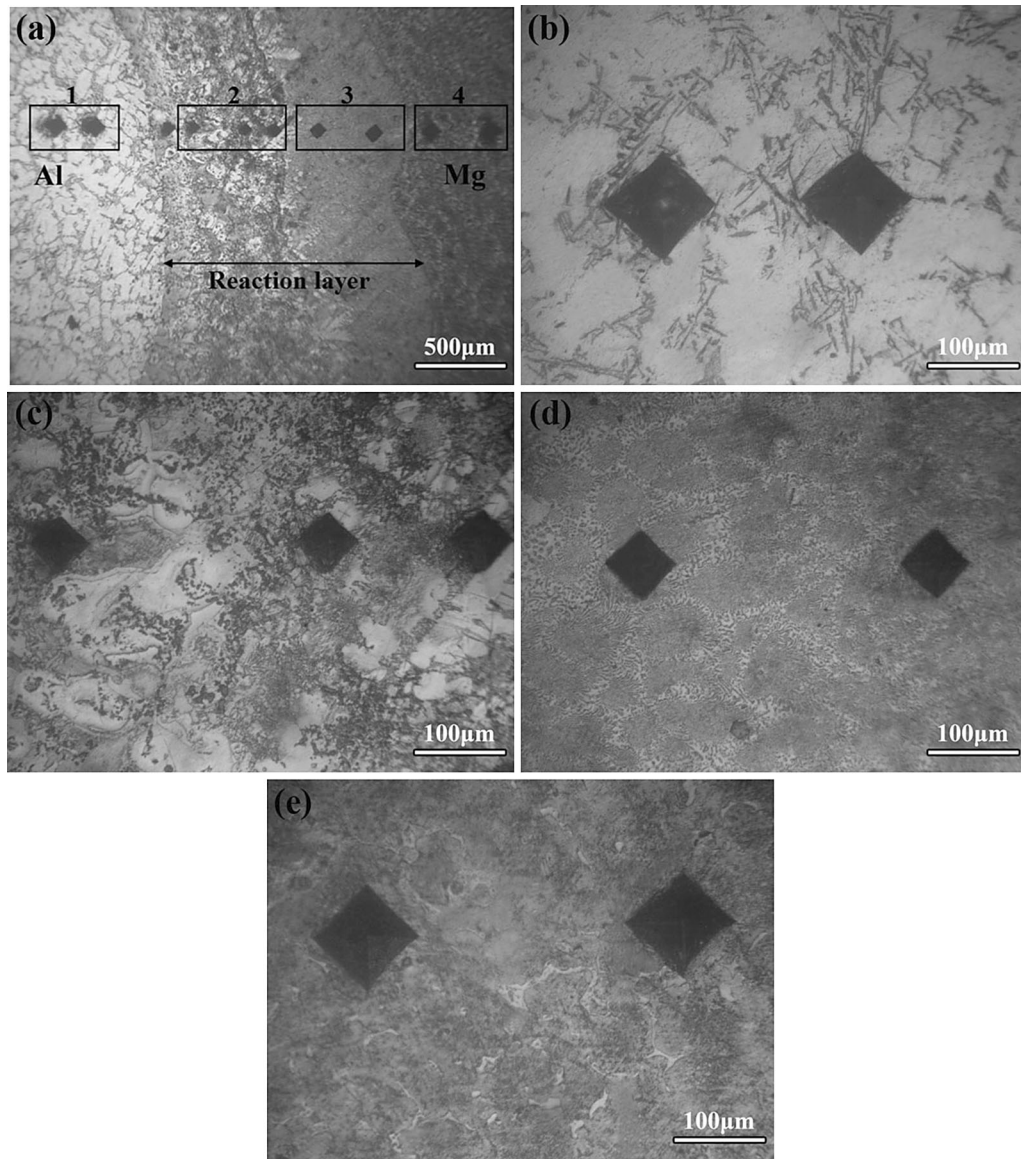Fig. 8—Schematic diagram of defect generation during the LFC process.

Fig. 10—Optical micrographs of the interfacial microstructures of the Al/Mg bimetallic castings obtained using LFC process after microhardness testing: (*a*) low-magnitude optical micrograph and (*b*) through (*e*) high-magnitude optical micrographs corresponding to areas 1, 2, 3, and 4, respectively.

investigations of process parameters and alloy interlayers,[37,38] aiming at the preparation of the reaction layer with an appropriate thickness.

IV. CONCLUSIONS

In the present work, the LFC process was used to prepare the Al/Mg bimetallic castings, and the interface characteristics of the reaction layer between the aluminum and magnesium produced by the LFC process were investigated. The obtained results can be summarized as follows.

1. The Al/Mg bimetallic castings were successfully fabricated using the LFC process. A uniform and compact interface between the aluminum and magnesium was formed, and the average thickness of the reaction layer reached approximately 1000 μm.

2. The reaction layer was mainly composed of the Al_3Mg_2 and $Al_{12}Mg_{17}$ intermetallic compounds, including three different layers such as the Al_3Mg_2 layer adjacent to the aluminum insert, the $Al_{12}Mg_{17}$ middle layer, and the $Al_{12}Mg_{17} + \delta$ eutectic layer adjacent to the magnesium base. Moreover, the Mg_2Si intermetallic compound was also found in the reaction layer.

3. The oxide film mainly containing C, O, and Mg elements, especially the C element, generated at the interface between the aluminum and magnesium. The decomposed residue of the foam pattern and the oxidations of magnesium and aluminum alloys as well as the reaction of the magnesium melt and the aluminum insert were responsible for the formation of the oxide film.

4. The microhardnesses at the interface were obviously higher than those of the magnesium and aluminum base metals. The Al_3Mg_2 layer had the highest microhardness in the reaction layer, while the $Al_{12}Mg_{17} + \delta$ eutectic showed a relatively lower microhardness compared to the Al_3Mg_2 and $Al_{12}Mg_{17}$ intermetallic compounds.

REFERENCES

1. W.M. Jiang, Z.T. Fan, X. Chen, B.J. Wang, and H.B. Wu: *Metall. Mater. Trans. A*, 2015, vol. 46A, pp. 1776–88.
2. Z.M. Li, Q.G. Wang, A.A. Luo, P.H. Fu, L.M. Peng, Y.X. Wang, and G.H. Wu: *Metall. Mater. Trans. A*, 2013, vol. 44A, pp. 5202–15.
3. H. Springer, A. Kostka, E.J. Payton, D. Raabe, A. Kaysser-Pyzalla, and G. Eggeler: *Acta Mater.*, 2011, vol. 59, pp. 1586–1600.
4. M. Marzouk, M. Jain, and S. Shankar: *Mater. Sci. Eng. A*, 2014, vol. 598, pp. 277–87.
5. K.J.M. Papis, B. Hallstedt, J.F. Loffler, and P.J. Uggowitzer: *Acta Mater.*, 2008, vol. 56, pp. 3036–43.
6. M. Paramsothy, N. Srikanth, and M. Gupta: *J. Alloys Compd.*, 2008, vol. 461, pp. 200–08.
7. M. Thirumurugan, S.A. Rao, S. Kumaran, and T.S. Rao: *J. Mater. Process. Technol.*, 2011, vol. 211, pp. 1637–42.
8. E Hajjari, M Divandari, SH Razavi, SM Emami, T Homma, and S Kamado: *J. Mater. Sci.*, 2011, vol. 46, pp. 6491–99.
9. W.M. Jiang, Z.T. Fan, D.J. Liu, D.F. Liao, X.P. Dong, and X.M. Zong: *Mater. Sci. Eng. A*, 2013, vol. 560, pp. 396–403.
10. P.M. Geffroy, M. Lakehal, J. Goni, E. Beaugnon, J.M. Heintz, and J.F. Silvain: *Metall. Mater. Trans. A*, 2006, vol. 37A, pp. 441–47.
11. X.J. Liu, S.H. Bhavnani, and R.A. Overfelt: *J. Mater. Process. Technol.*, 2007, vol. 182, pp. 333–42.
12. W.M. Jiang, Z.T. Fan, D.J. Liu, D.F. Liao, Z. Zhao, X.P. Dong, and H.B. Wu: *Int. J. Cast Met. Res.*, 2012, vol. 25, pp. 47–52.
13. Z.L. Liu, J.Y. Hu, Q.D. Wang, W.J. Ding, Y.P. Zhu, Y.Z. Lu, and W.Z. Chen: *J. Mater. Process. Technol.*, 2002, vol. 120, pp. 94–100.
14. M.R. Barone and D.A. Caulk: *Int. J. Heat Mass Transfer*, 2005, vol. 48, pp. 4132–49.
15. M.M. Hejazi, M. Divandari, and E. Taghaddos: *Mater. Des.*, 2009, vol. 30, pp. 1085–92.
16. M. Divandari and A.R. Vahid Golpayegani: *Mater. Des.*, 2009, vol. 30, pp. 3279–85.
17. K.H. Choe, K.S. Park, B.H. Kang, G.S. Cho, K.Y. Kim, K.W. Lee, M.H. Kim, A. Ikenaga, and S. Koroyasu: *J. Mater. Sci. Technol.*, 2008, vol. 24, pp. 60–64.
18. E. Hajjari, M. Divandari, S.H. Razavi, T. Homma, and S. Kamado: *Metall. Mater. Trans. A*, 2012, vol. 43A, pp. 4667–77.
19. A. Kostka, R.S. Coelho, J. dos Santos, and A.R. Pyzalla: *Scripta Mater.*, 2009, vol. 60, pp. 953–56.
20. H. Zhang, Y.Q. Chen, and A.A. Luo: *Scripta Mater.*, 2014, vol. 86, pp. 52–55.
21. J. Wang, Y.J. Li, P. Liu, and H.R. Geng: *J. Mater. Process. Technol.*, 2008, vol. 205, pp. 146–50.
22. M. Gao, S.W. Mei, X.Y. Li, and X.Y. Zeng: *Scripta Mater.*, 2012, vol. 67, pp. 193–96.
23. S.M. Emami, M. Divandari, E. Hajjari, and H. Arabi: *Int. J. Cast Met. Res.*, 2013, vol. 26, pp. 43–50.
24. K.A. Guler, A. Kisasoz, and A. Karaaslan: *Mater. Test.*, 2014, vol. 56, pp. 700–02.
25. U.R. Kattner and T.B. Massalski: *Binary Alloy Phase Diagrams*, ASM International, Material Park, 1990.
26. E. Hajjari, M. Divandari, S.H. Razavi, T. Homma, and S. Kamado: *Intermetallics*, 2012, vol. 23, pp. 182–86.
27. D. Singh, C. Suryanarayana, L. Mertus, and R.H. Chen: *Intermetallics*, 2003, vol. 11, pp. 373–76.
28. W.M. Jiang, Z.T. Fan, D.F. Liao, D.J. Liu, Z. Zhao, and X.P. Dong: *Mater. Des.*, 2011, vol. 32, pp. 926–34.
29. J. Campbell: *Casting*, 2nd ed., Butterworth-Heinemann, Oxford, 2003.
30. A.R. Mirak, M. Divandari, S.M.A. Boutorabi, and J. Campbell: *Int. J. Cast Met. Res.*, 2007, vol. 20, pp. 215–20.
31. C.R. Werrett, D.R. Pyke, and A.K. Bhattacharya: *Surf. Interface Anal.*, 1997, vol. 25, pp. 809–16.
32. P. Liu, Y. Li, H. Geng, and J. Wang: *Mater. Lett.*, 2007, vol. 61, pp. 1288–91.
33. Y.S. Sato, S. Hwan, C. Park, M. Michiuchi, and H. Kokawa: *Scripta Mater.*, 2004, vol. 50, pp. 1233–36.
34. D. Dietrich, D. Nickel, M. Krause, T. Lampke, M.P. Coleman, and V. Randle: *J. Mater. Sci.*, 2011, vol. 46, pp. 357–64.
35. Y.Y. Wang, G.Q. Luo, J. Zhang, Q. Shen, and L.M. Zhang: *J. Alloys Compd.*, 2012, vol. 541, pp. 458–61.
36. L.M. Zhao and Z.D. Zhang: *Scripta Mater.*, 2008, vol. 58, pp. 283–86.
37. L.M. Liu, X.J. Liu, and S.H. Liu: *Scripta Mater.*, 2006, vol. 55, pp. 383–86.
38. Y.Y. Wang, G.Q. Luo, J. Zhang, Q. Shen, and L.M. Zhang: *Mater. Sci. Eng. A*, 2013, vol. 559, pp. 868–74.